2006

Tight-binding study of thermal expansions for Mo3Si

Ning Ma

Bernard R. Cooper

Bruce S. Kang

Tight-binding study of thermal expansions for Mo_3Si

Ning Ma[a] and Bernard R. Cooper
Department of Physics, West Virginia University, Morgantown, West Virginia 26506

Bruce S. Kang
Mechanics and Aerospace Engineering Department, West Virginia University, Morgantown, West Virginia 26506

(Received 17 January 2005; accepted 23 January 2006; published online 8 March 2006)

We implemented a tight-binding parameter extraction scheme that is suitable for the modeling of intermetallic alloy systems. Using Mo_3Si as an example, we obtained the Slater-Koster tight-binding parameters directly from results of full-potential linear muffin-tin orbital calculation by using a modification of the approach of McMahan and Klepeis [Phys. Rev. B **56**, 12250 (1997)]. The transferability and accuracy of these parameters were tested against *ab initio* results. Augmented by a fitted repulsive energy contribution that takes the form of embedded atom potential, the tight-binding total energy method was applied in Monte Carlo simulations to compute the coefficients of thermal expansion for Mo_3Si. © *2006 American Institute of Physics*.
[DOI: 10.1063/1.2178401]

I. INTRODUCTION

Formulated in the classic work of Slater and Koster[1] half a century ago, tight-binding (TB) methods have experienced a renewed popularity in the recent literature. In contrast to the original method, which was mainly an experimental data interpolation scheme, modern TB methods have been developed to predict electronic structure with accuracy comparable to first-principles electronic methods. The success of TB is due not only to its advantage of theoretical simplicity and numerical efficiency, but also to its real-space approach, which makes it widely applicable to systems that lack perfect crystalline symmetry (e.g., defects, impurities, surfaces, and interfaces). Unlike other classical-potential-based empirical methods, TB is based on a quantum-mechanical formulation and is therefore more appropriate to explore the quantum nature of chemical bonding properties and to describe complicated materials such as transition metals.

In the past, TB method has achieved considerable success in the modeling of single elements[2] and some semiconducting alloy systems. However, the application of TB in intermetallic alloy systems[3,4] has been very limited, primarily due to the lack of quality TB parameters. The conventional means to obtain TB parameters is to fit the TB energy bands to those obtained either from first-principles theoretical calculations or experimental results. The numerical fitting procedure, which performs the standard nonlinear minimization on the merit function, works well for single element materials where the number of independent parameters is relatively small. In contrast, a typical binary intermetallic material requires over 300 independent parameters. To fit so many parameters simultaneously is prohibitively tedious, and the merit function can easily be trapped into local minima, resulting in unphysical TB parameters that produce energy bands having little resemblance to the original ones.

In this article, we present a TB parameter extraction scheme which avoids the aforementioned difficulties, and is particularly suitable for the modeling of intermetallic alloy materials. In this scheme, we first follow the method of McMahan and Klepeis[5,6] to extract the intersite Slater-Koster (SK) parameters *directly* from the Hamiltonian and overlap matrices, which are computed by the first-principles full-potential linear muffin-tin orbital (FP-LMTO) method.[7,8] Precalibration of energy is applied on Hamiltonian matrices to ensure transferability. We obtain the on-site SK parameters based on a simplifying assumption about the crystal fields. Finally, we augment the band energy with a repulsive contribution to account for the difference of the first-principles total energy and TB band energy. We note in passing that the idea of obtaining TB parameters directly from first-principles calculation actually dates back to Andersen and Jepsen,[9] and has been continued by other groups.[10] The application to intermetallic alloy materials has been performed by Djajaputra and Cooper for NiAl,[8] where the Hamiltonian matrix elements were used as input to real-space calculation of the local density of states (DOS) using the recursion method.

To be specific, we choose A15 cubic Mo_3Si (Fig. 1) as our example material. A number of molybdenum-silicide alloys are being developed as high-temperature (>1000 °C)

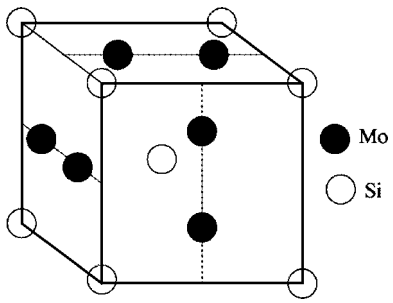

FIG. 1. The cubic A15 structure for Mo_3Si: The Mo atoms (black circles) form lines bisecting the cubic surfaces, and Si atoms (white circles) occupy the bcc lattice.

[a]Author to whom correspondence should be addressed; electronic mail: n_ma12@yahoo.com

structural materials for many important fossil energy applications.[11] A promising alloy system currently under substantial investigation[12] is the ternary phase $Mo_5SiB_2(T_2)$–Mo_3Si–Mo. It is known that the anisotropy and incompatibility of the thermal expansions of the ternary phase field causes thermal stress and this can lead to microcracking. To tailor the mechanical properties and oxidation resistance within the ternary phase field, it is highly desirable to be able to predict the off-stoichiometry temperature dependence of the thermal expansions of the three components up to very high temperatures. In this paper we will use Monte Carlo simulation based on TB method to predict the temperature-dependent coefficients of thermal expansion (CTE) for Mo_3Si.

In the following sections, we shall first present a detailed description of the method in Sec. II, then the test results of accuracy and transferability of the TB parameters will be presented in Sec. III, which are followed by the Monte Carlo simulation results for CTE in Sec. IV, and finally a brief summary in Sec. V.

II. METHODOLOGY

As usual, we separate the total energy into TB band energy and repulsive potential,

$$E_{\text{tot}} = E_{\text{band}} + E_{\text{rep}}. \tag{1}$$

The above separation of total energy involves some arbitrariness. In some TB total energy schemes (notably Cohen *et al.*[13]), the repulsive potential is entirely absorbed by the band energy as a chemical potential shift of the site energies. While this treatment simplifies the expression for the total energy, it obscures the physical meaning of each individual component. We shall keep both terms in the total energy expression. The issue of the energy separation will be addressed later in the procedure of energy calibration.

A. The band energy

In the nonorthogonal TB model, one computes the Hamiltonian and overlap matrices, H and S, and solves the generalized eigenproblem,

$$(H - \varepsilon_i S)\psi_i = 0. \tag{2}$$

The band energy is obtained by summing up all the energy eigenvalues weighted by Fermi distribution function,

$$E_{\text{band}} = \sum_i \varepsilon_i f(\varepsilon_i). \tag{3}$$

Based on the two center approximation, Slater and Koster[1] expressed the Hamiltonian and overlap matrix elements as linear combinations of a set of parameters known as SK parameters. For example, an intersite ($R \neq 0$) Hamiltonian or overlap matrix element may be written as (here we used the McMahan convention[5])

$$\langle 0lm|H|\mathbf{R}l'm'\rangle = \sum_\mu g_\mu(lm,l'm',\hat{\mathbf{R}})t_{ll'\mu}(R) \tag{4}$$

and

$$\langle 0lm|S|\mathbf{R}l'm'\rangle = \sum_\mu g_\mu(lm,l'm',\hat{\mathbf{R}})s_{ll'\mu}(R), \tag{5}$$

where g_μ's are the linear coefficients that describe the geometric alignment of the participating atomic orbitals, and $t_{ll'\mu}$'s and $s_{ll'\mu}$'s are the Hamiltonian and overlap SK parameters that depend only upon the intersite distance R.

The inverse problem, namely, to determine SK parameters from given Hamiltonian and overlap matrices, has been studied by McMahan and Klepeis.[5,6] They found an orthogonality relationship among the g_μ's that can be used to invert Eqs. (4) and (5),

$$t_{ll'\mu}(R) = \frac{1}{2 - \delta_{\mu\sigma_{m,m'}}} \sum g_\mu(lm,l'm',\hat{\mathbf{R}})\langle 0lm|H|\mathbf{R}l'm'\rangle, \tag{6}$$

$$s_{ll'\mu}(R) = \frac{1}{2 - \delta_{\mu\sigma_{m,m'}}} \sum g_\mu(lm,l'm',\hat{\mathbf{R}})\langle 0lm|S|\mathbf{R}l'm'\rangle. \tag{7}$$

Thus, the procedure of obtaining intersite SK parameters is made straightforward: One first computes the k-space Hamiltonian and overlap matrices for the material using first-principles method. The matrices are then anti-Fourier transformed into the real space. Using Eqs. (6) and (7), the intersite TB parameters for a particular structure are thus obtained. In our implementation, we have used the FP-LMTO (Ref. 7) method with single-kappa minimal basis to deduce the TB parameters. The kappa decay parameter is set to be −0.4, and the muffin-tin (MT) radii are 2.1912 bohr for Mo and 2.4560 bohr for Si, respectively. The TB basis consists of Mo's 5s, 4p, and 3d orbitals and Si's 3s, 3p, and 3d orbitals.

The crucial difference between this procedure and conventional schemes through parameter fitting is the following. Conventional schemes start with the total energy and band structure, which are essentially the *eigenvalues* of the Hamiltonian and overlap matrices. One then proceeds to probe the TB parameter space for the set that will generate these eigenvalues. From a mathematics point of view, it is easy to have different sets of TB parameters, or different TB matrices, that produce the same set of eigenvalues. Therefore, the results of a conventional scheme are usually not unique, and are dependent on initial trial parameters. In contrast, this *ab initio* based parameter retrieving scheme starts directly from the *matrix elements* themselves (rather than their derived *eigenvalues*). The subsequent procedure of inverting these matrix elements to obtain their corresponding TB parameters will guarantee the results to be unique. Thus, by abandoning the eigenvalues and by working directly with the physically more informative matrix elements, we eliminate the uncertainties inherited from numerical fitting procedures.

When relating the intersite parameters prepared at different lattice volumes, some caution must be taken. This is because the SK parametrization implicitly assumes a fixed set of basis. However, the FP-LMTO method searches for the optimal basis that minimizes the density functional which is not fixed. In practice, we find that fixing the MT radii usually results in a relatively fixed basis. This can be seen from Fig. 2, where the overlap SK parameters $s(R)$ obtained at a series

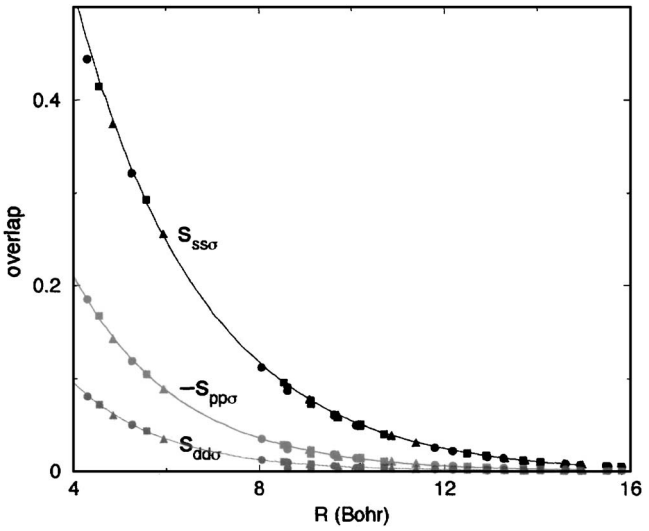

FIG. 2. The overlap intersite parameters $s(R)$ obtained at various lattice constants: circles (a_0=8.608 bohr), squares (a_0=9.121 bohr), and triangles (a_0=9.707 bohr).

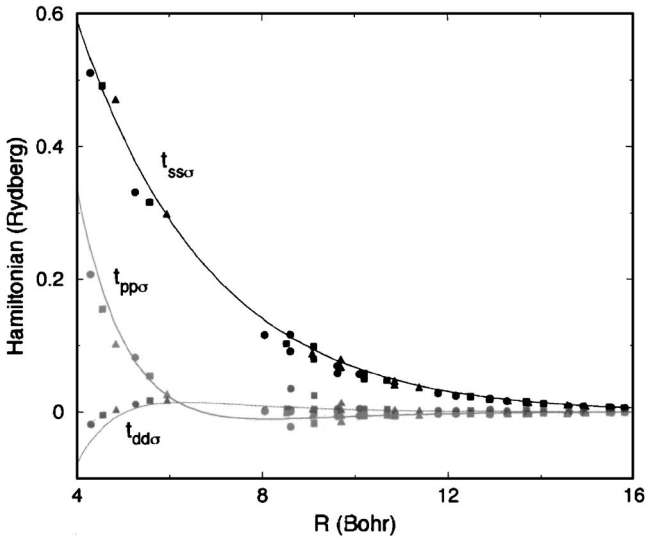

FIG. 4. The Hamiltonian intersite parameters $t(R)$, after the calibration Eq. (8), obtained at various lattice constants: circles (a_0=8.608 bohr), squares (a_0=9.121 bohr), and triangles (a_0=9.707 bohr).

of lattice volumes collapse into a common curve. We note in passing that the authors in Ref. 1 performed an explicit unitary rotation transformation on the TB orbital basis to ensure a fixed set of overlap parameters. In that case, the issues of transferability were entirely relegated to the transformed Hamiltonian parameters.

In contrast to Fig. 2, the Hamiltonian parameters obtained at different lattice volumes show noticeable disagreement (see Fig. 3). In many other implementations, explicit environment dependent TB parametrization schemes[14] have been invoked to resolve this discrepancy. Here, however, we are aware that the discrepancy only occurs in Hamiltonian parameters and not in overlap parameters. We therefore believe that the cause of discrepancy is mostly due to the arbitrariness of the total energy separation mentioned at the beginning of Sec. II. In FP-LMTO calculation, the energy reference of the band energy term is not fixed. This causes

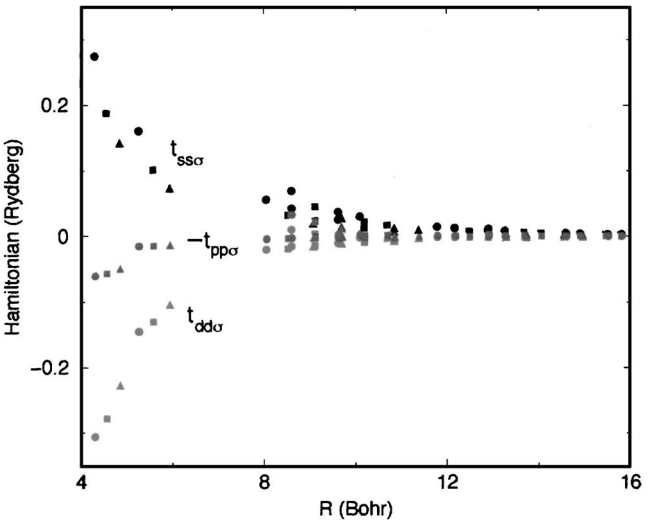

FIG. 3. The Hamiltonian intersite parameters $t(R)$ obtained at various lattice constants: circles (a_0=8.608 bohr), squares (a_0=9.121 bohr), and triangles (a_0=9.707 bohr).

arbitrary separation of total energy in Eq. (1) when the calculations are performed at different lattice volumes. Therefore, it is necessary to calibrate the energy references for the Hamiltonian matrices prior to SK parameter extraction.

To perform the energy calibration, we assume the lowest energy level of the core electron ε_{1s} to be unaffected by the variations of lattice volume. Its calculated value is then used as a reference to measure the corresponding potential matrix. This leads to the following transformation on the Hamiltonian parameters:

$$\tilde{t} = t(a) - \Delta\varepsilon_{1s}(a)s, \tag{8}$$

where a is the lattice constant at which the Hamiltonian parameters are obtained. After the calibration, the transformed Hamiltonian parameters are plotted in Fig. 4, where an improved agreement over Fig. 3 is apparent.

We fit the overlap and calibrated Hamiltonian SK parameters into the following form:

$$t(R) = (a_0 + a_1 R)e^{-a_2 R}, \tag{9}$$

$$s(R) = (b_0 + b_1 R)e^{-b_2 R}. \tag{10}$$

Results of intersite SK parameters are tabulated in Table I.

We now turn to the on-site (R=0) matrix elements. The on-site overlap matrix is simply unity if the TB orbitals are properly orthonormalized. For the on-site Hamiltonian matrix, we assume that the off-diagonal mixings produced by crystal field potentials are negligibly small (they are usually three orders of magnitude smaller than the diagonal terms). Thus the remaining problem is to determine the diagonal Hamiltonian matrix elements, which are the site energies of the corresponding orbital plus crystal field corrections. In contrast to the case of intersite SK parameters, neither the site energy nor the crystal field correction can be directly extracted from the FP-LMTO results. It was found in Ref. 1 that certain sums of these parameters remain directly computable. However, these sums are structure dependent, i.e., nontransferable. To obtain a transferable set of TB on-site

TABLE I. Intersite SK parameters obtained for Mo_3Si. All energies are in rydberg (1 Ry=13.6 eV) and all lengths are in bohr.

	Type	a_0	a_1	a_2		Type	b_0	b_1	b_2
$t_{ss\sigma}$	Mo–Mo	2.394 958	−0.100 570	0.302 562	$s_{ss\sigma}$	Mo–Mo	2.184 894	−0.088 982	0.313 869
$t_{sp\sigma}$	Mo–Mo	1.647 918	−0.515 773	0.484 199	$s_{sp\sigma}$	Mo–Mo	−1.339 309	0.048 700	0.336 927
$t_{sd\sigma}$	Mo–Mo	0.348 992	−0.017 912	0.232 544	$s_{sd\sigma}$	Mo–Mo	0.619 274	−0.027 074	0.319 371
$t_{pp\sigma}$	Mo–Mo	13.018 420	−1.945 851	0.682 066	$s_{pp\sigma}$	Mo–Mo	−1.016 580	0.042 324	0.363 162
$t_{pp\pi}$	Mo–Mo	−3.348 075	0.628 334	0.693 988	$s_{pp\pi}$	Mo–Mo	1.031 993	0.000 000	0.566 343
$t_{pd\sigma}$	Mo–Mo	−10.525 070	1.618 473	0.719 870	$s_{pd\sigma}$	Mo–Mo	0.686 851	−0.035 697	0.372 834
$t_{pd\pi}$	Mo–Mo	8.390 044	−1.585 033	0.811 952	$s_{pd\pi}$	Mo–Mo	−1.196 728	0.000 000	0.599 605
$t_{dd\sigma}$	Mo–Mo	−9.190 844	1.808 697	0.804 322	$s_{dd\sigma}$	Mo–Mo	0.599 902	−0.032 720	0.415 515
$t_{dd\pi}$	Mo–Mo	17.143 060	−3.624 188	0.922 667	$s_{dd\pi}$	Mo–Mo	−1.090 491	0.061 161	0.528 445
$t_{dd\delta}$	Mo–Mo	0.055 455	−0.004 009	0.281 229	$s_{dd\delta}$	Mo–Mo	0.764 905	−0.000 000	0.746 754
$t_{ss\sigma}$	Si–Si	1.486 036	−0.065 194	0.272 349	$s_{ss\sigma}$	Si–Si	2.440 944	−0.023 419	0.381 072
$t_{sp\sigma}$	Si–Si	−1.225 072	0.055 517	0.256 089	$s_{sp\sigma}$	Si–Si	−2.248 722	−0.000 000	0.392 436
$t_{sd\sigma}$	Si–Si	0.482 761	−0.022 647	0.232 424	$s_{sd\sigma}$	Si–Si	1.268 798	−0.000 000	0.407 302
$t_{pp\sigma}$	Si–Si	−1.043 286	0.048 141	0.242 436	$s_{pp\sigma}$	Si–Si	−2.132 760	−0.000 000	0.400 005
$t_{pp\pi}$	Si–Si	2.150 527	0.000 000	0.512 786	$s_{pp\pi}$	Si–Si	1.254 798	−0.000 000	0.481 017
$t_{pd\sigma}$	Si–Si	0.467 511	−0.022 066	0.227 411	$s_{pd\sigma}$	Si–Si	1.632 812	−0.000 000	0.441 305
$t_{pd\pi}$	Si–Si	−1.925 275	0.070 190	0.465 273	$s_{pd\pi}$	Si–Si	−1.216 405	0.000 000	0.495 945
$t_{dd\sigma}$	Si–Si	0.298 144	−0.014 322	0.237 251	$s_{dd\sigma}$	Si–Si	1.830 145	−0.000 000	0.506 001
$t_{dd\pi}$	Si–Si	−1.360 566	0.076 854	0.391 682	$s_{dd\pi}$	Si–Si	−1.889 483	0.000 000	0.561 865
$t_{dd\delta}$	Si–Si	3.581 653	−0.000 000	0.773 526	$s_{dd\delta}$	Si–Si	0.507 738	0.000 000	0.584 228
$t_{ss\sigma}$	Mo–Si	1.793 413	−0.086 824	0.270 998	$s_{ss\sigma}$	Mo–Si	2.165 409	−0.086 853	0.319 271
$t_{sp\sigma}$	Mo–Si	−1.848 177	0.087 301	0.282 404	$s_{sp\sigma}$	Mo–Si	−1.786 073	0.076 326	0.305 213
$t_{sd\sigma}$	Mo–Si	1.807 832	0.000 000	0.420 076	$s_{sd\sigma}$	Mo–Si	0.944 423	−0.043 515	0.305 460
$t_{ps\sigma}$	Mo–Si	−8.851 011	1.956 687	0.620 730	$s_{ps\sigma}$	Mo–Si	1.386 815	−0.042 992	0.354 105
$t_{pp\sigma}$	Mo–Si	10.807 530	−2.136 544	0.632 395	$s_{pp\sigma}$	Mo–Si	−1.412 994	0.037 192	0.373 450
$t_{pp\pi}$	Mo–Si	0.137 332	−0.007 643	0.222 102	$s_{pp\pi}$	Mo–Si	1.418 044	−0.000 000	0.545 895
$t_{pd\sigma}$	Mo–Si	−14.657 200	2.668 261	0.745 364	$s_{pd\sigma}$	Mo–Si	1.368 426	0.000 000	0.468 398
$t_{pd\pi}$	Mo–Si	18.359 460	−3.801 283	0.845 518	$s_{pd\pi}$	Mo–Si	−1.737 418	0.000 000	0.582 592
$t_{ds\sigma}$	Mo–Si	0.249 246	−0.012 073	0.223 387	$s_{ds\sigma}$	Mo–Si	0.718 059	−0.024 245	0.356 363
$t_{dp\sigma}$	Mo–Si	−0.413 028	0.016 745	0.291 659	$s_{dp\sigma}$	Mo–Si	−0.676 139	0.031 602	0.332 821
$t_{dp\pi}$	Mo–Si	0.382 101	−0.024 287	0.293 396	$s_{dp\pi}$	Mo–Si	1.420 029	−0.000 000	0.564 451
$t_{dd\sigma}$	Mo–Si	1.229 843	−0.000 000	0.529 222	$s_{dd\sigma}$	Mo–Si	0.941 093	−0.034 755	0.438 201
$t_{dd\pi}$	Mo–Si	−0.483 843	0.032 590	0.315 845	$s_{dd\pi}$	Mo–Si	−2.255 753	0.000 000	0.639 634
$t_{dd\delta}$	Mo–Si	0.306 421	−0.022 542	0.420 954	$s_{dd\delta}$	Mo–Si	0.989 172	0.000 000	0.711 395

parameters, we used an alternative scheme described as the following: First, we approximate the crystal field potential as a superposition of a mesh of delta functions situated at atomic sites. Thus the corrections to the site energy are particularly easy to evaluate, and the resulting diagonal matrix elements now take the form

$$e_{lm} = e_l^0 + \sum_{\mathbf{R}\neq 0} h|\psi_{lm}(\mathbf{R})|^2. \tag{11}$$

Here e_l^0 is the site energy, h is the coefficient of the delta functions, or the strength of the crystal fields, and ψ_{lm} is the wave function of the orbital. The summation is carried out over all atomic sites excluding the hosting site. For R much larger than the MT radius, we can replace $\psi_{lm}(\mathbf{R})$ with its asymptotic behavior. It is parametrized in the following Gaussian form:

$$|\psi_{l,m}(\mathbf{R})|^2 = c_0 e^{-(R-c_1)^2/c_2^2}|Y_m^l(\hat{\mathbf{R}})|^2. \tag{12}$$

In this form, orbitals that differ only in magnetic number share a common radial part. This enables us to significantly reduce the number of parameters in the fitting while still retaining the correct angular dependence of these orbitals.

A few remarks are in order: First, the fitting is individually performed for each orbital set having a common angular momentum. This fitting is to be contrasted to the conventional fitting scheme in that we are fitting directly to the diagonal matrix elements one at a time, rather than fitting to the entire set of eigenvalues or the band structure. Therefore, the results are still unique. Second, energy calibration is necessary to obtain correctly behaved on-site parameters. To see this, we note that Eq. (11) suggests that the volume dependence of e_{lm} vanish at large lattice volume, since the crystal field corrections eventually vanish. Without appropriate calibration, the computed diagonal Hamiltonian matrix elements may not behave this way due to the floating energy reference point.

B. The repulsive potential

The TB band energy is purely attractive. To explain the bonding behavior, we need a repulsive contribution that accounts for the ion-ion repulsions and the correction for the overcounting of electron-electron interactions.

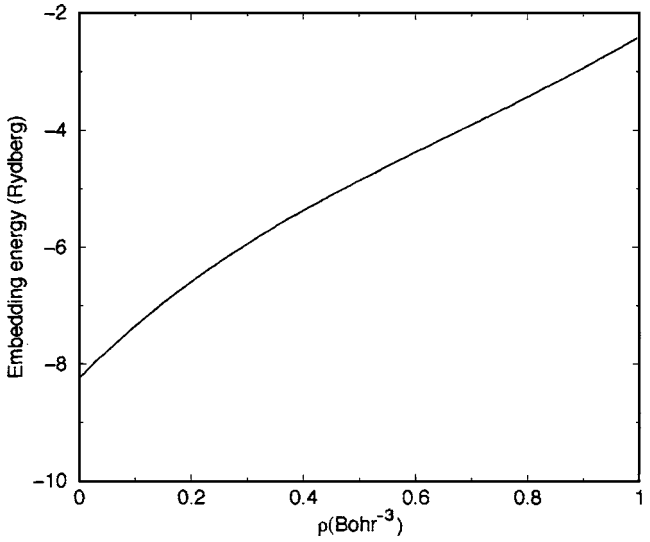

FIG. 5. The embedding function for Mo_3Si. With lattice constant of Mo_3Si varied from 8.24 to 9.52 bohr, the ranges of ρ_{Mo} and ρ_{Si} are 0.595–0.246 and 0.658–0.273 bohr^{-3}, respectively.

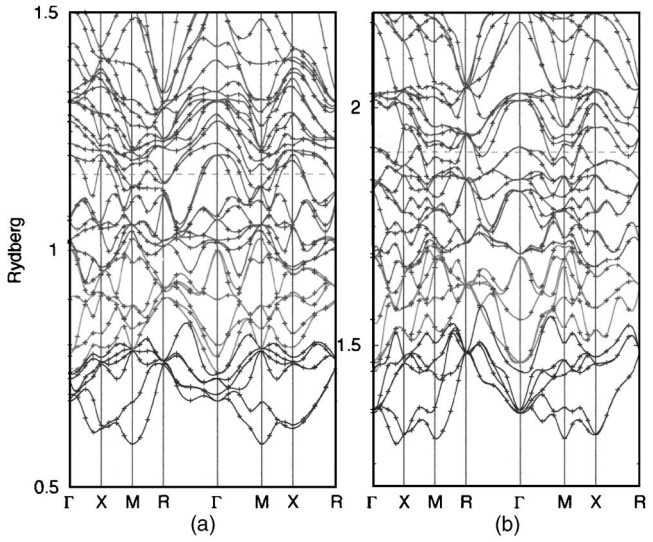

FIG. 6. Calculated band structures for A15 Mo_3Si, using (a) FP-LMTO with single-kappa basis and (b) TB method. Shown in the figure are Mo's 5*s*, (partial) 3*d*, and Si's 3*p* bands. The dashed lines are the Fermi levels.

We implement the repulsive potential in an embedded atom method (EAM) scheme,[15] where the repulsive energy is a sum of embedding energies that depend on the local electron densities at each atomic site,

$$E_{\text{rep}} = \sum_{\mathbf{R}} f(\rho(\mathbf{R})). \tag{13}$$

The form of the embedding function f is unknown, and is determined by fitting. The electron density ρ at site $\mathbf{R}$ is taken to be a linear superposition of first-principles computed electron densities of corresponding isolated atoms,

$$\rho(\mathbf{R}) = \sum_{\mathbf{R}' \neq \mathbf{R}} \rho^0(\alpha|\mathbf{R}' - \mathbf{R}|). \tag{14}$$

In practice, we find that the use of bare atomic density superposition yields a repulsive contribution that is often too short ranged. Therefore, we introduce a scaling factor α for interatomic distance in Eq. (14), and we find $\alpha = 0.74$ gives the optimal results. The need of a longer-ranged density may be explained by the presence of the long-range Coulomb interactions.

Once the local densities at all sites are available, we fit the embedding function f in Eq. (13) to a piecewise third-order polynomial function. The left-hand side of Eq. (13) is taken to be the difference between first-principles FP-LMTO total energy and TB band energy. The database contains uniform contractions and expansions of the lattice about the equilibrium volume. In the FP-LMTO calculation, we treat the 4*p* semicore electrons of Mo as valence electrons in a separate energy window (to be distinguished from 5*p* electrons), and use four-kappa linked basis to describe each valence orbital to achieve maximum accuracy. The four kappas are set to be −0.9, 0.3, 1.2, and −1.2, respectively (the last kappa is used exclusively in the second energy window). The resulting embedding function is shown in Fig. 5. Since our goal is to estimate thermal expansions that require only small deviations about the equilibrium structure, we find a common embedding function for Mo and Si is sufficient.

III. TESTS OF PARAMETERS

In this section, we discuss various tests on our parameters for their accuracy and transferability.

A. Accuracy tests for small lattice deviations around A15 Mo_3Si

To test the accuracy of the parameters on A15 Mo_3Si and some deviations from that structure, we first calculated the band structure and density of states for A15 Mo_3Si at the equilibrium lattice volume, and compared the results with those obtained using first-principles FP-LMTO method. In the FP-LMTO method, we used a single-kappa basis that was originally used in developing the TB parameters. The purpose here is to provide a measure of the overall accuracy of the two center approximation plus the crystal field effects included in the TB parametrization scheme. The results are shown in Figs. 6 and 7, respectively. In the band-structure calculation, the agreement between the two methods are generally good for bands below and around the Fermi level. Farther above the Fermi level the accuracy becomes questionable, which is a usual problem of this and many other electronic structure methods. In Fig. 7 qualitative agreement on DOS is maintained, despite several discrepancies about the precise positions and weights of the DOS peaks predicted by both methods.

Next, we conducted some elastic moduli calculations using both the first-principles FP-LMTO method and the TB total energy formula. In this case, we used four-kappa linked basis in FP-LMTO method and separate energy window treatment for Mo's semicore 4*p* electrons, to achieve maximum accuracy. For A15 cubic structure, there are three independent elastic moduli: c_{11}, c_{12}, and c_{44}. These elastic moduli were obtained by applying the following three types of small strains to the equilibrium lattice and determining the resulting change in the total energy:[16]

- uniform volume expansion and contraction;

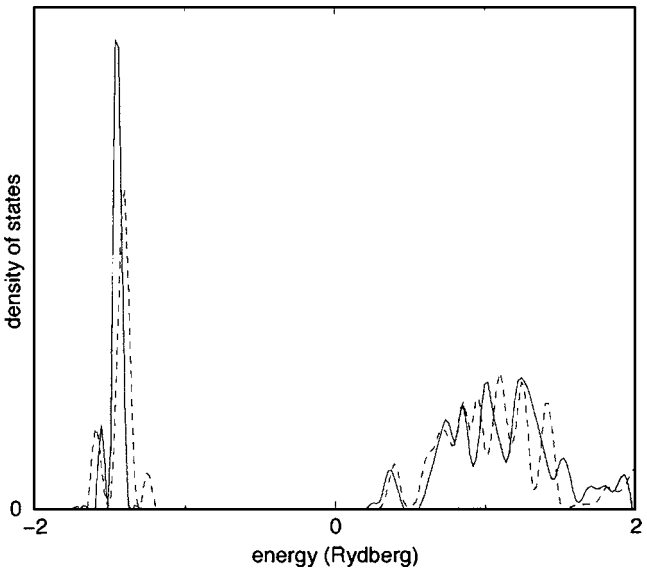

FIG. 7. Calculated density of states for A15 Mo_3Si, using FP-LMTO with single-kappa basis (solid line) and TB method (dashed line). The TB results have been shifted in energy in order to be compared with FP-LMTO results.

- volume-conserving tetragonal shear;
- volume-conserving monoclinic strain.

The above three strains will correspond to $c_{11}+2c_{12}$, $c_{11}-c_{12}$, and c_{44}, respectively. The converted elastic moduli are compared and tabulated in Table II. Note that in the tetragonal and monoclinic distortions, we have not performed any internal relaxations. Therefore, the calculated results would give upper bounds for $c_{11}-c_{12}$ and c_{44}.

For tetragonal strain, there is a large discrepancy between the TB method and FP-LMTO method. We believe the discrepancy mainly originates from the assumption of direct superposition of the atomic density. Had the atomic density been allowed to relax, for example, to have an anisotropic decay rate according to the applied strain, the resulting $c_{11}-c_{12}$ should yield a closer value as predicted by FP-LMTO. This atomic density relaxation effect is less prominent under the more isotropic monoclinic strain, where better agreement of c_{44} between the two methods is seen.

Finally, in addition to calculating the elastic moduli, which are related to the zone center acoustic-phonon modes, we also estimated the energy associated with an optical-phonon mode. In this mode, the nearest Mo pairs are oscillating with respect to each other, while Si atoms are fixed in space. Clearly this is a normal vibrational mode since it preserves many symmetries of the original lattice. We computed the total energy change and fit it to a quadratic form of the vibration amplitude. The coefficient of the quadratic form is related to the mode frequency as $m\omega^2/2$. The mode frequency is predicted to be 15.72 and 17.03 THz by TB and FP-LMTO, respectively.

TABLE II. Elastic moduli (in GPa) for Mo_3Si calculated by FP-LMTO and TB methods.

	FP-LMTO	TB
c_{11}	539	939
c_{12}	147	42
c_{44}	118	220

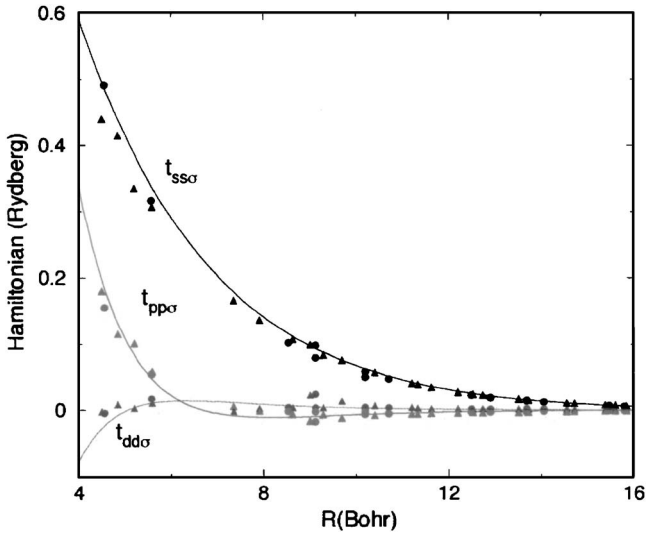

FIG. 8. The comparison of two sets of parameters for Mo. The circles are obtained for A15 Mo_3Si, and the triangles are obtained for bcc Mo. The lines are fits to $(a_0+a_1x)e^{-a_2x}$.

B. Transferability tests of TB parameters

In this section, we shall address the transferability issues, namely, how the obtained SK TB parameters can be applied to crystal structures other than the A15 Mo_3Si. We shall limit our discussion to those of the TB parameters only. In this work, no efforts have been made to make the EAM parameters transferable.

In the first test, we consider pure Mo (bcc) and pure Si [cubic diamond (cd)]. For these two structures, we independently develop another set of intersite SK parameters using the same scheme (with the same FP-LMTO parameters). The newly developed SK parameters are then compared to those originally developed for A15 Mo_3Si in Figs. 8 (bcc Mo) and 9(cd Si), respectively. We see good agreement in Mo parameters. This demonstrates the uniqueness of the TB parameters resulting from our scheme. However, there are significant discrepancies in Si parameters. To explain the poor transferability for Si, we note that in developing the TB parameters for cd Si, we have used a single-kappa minimal basis. While such a basis set works well for close-packed bcc and A15 structures, it can be very bad for the open structures, in particular, for the cd Si. In addition, we noticed that the equilibrium nearest Si–Si distance is about 4.2 Å in Mo_3Si while it is about 2.3 Å in cd Si.

As an additional measure, we have considered two other crystal structures with the same Mo_3Si composition: $L1_2$ and $D0_3$. We calculated their band structures and compared them with those obtained from first-principles FP-LMTO (using single-kappa basis) in Figs. 10 and 11. Consistent agreement is seen.

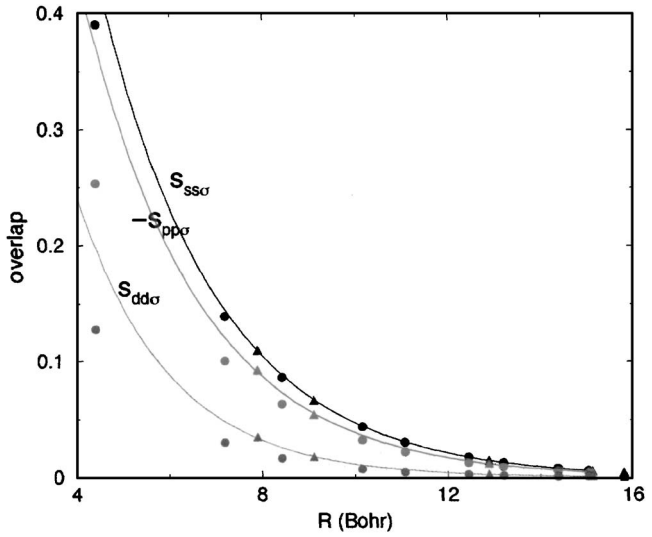

FIG. 9. The comparison of two sets of parameters for Si. The circles are obtained for A15 Mo_3Si, and the triangles are obtained for cubic diamond Si. The lines are fits to $(a_0+a_1x)e^{-a_2x}$.

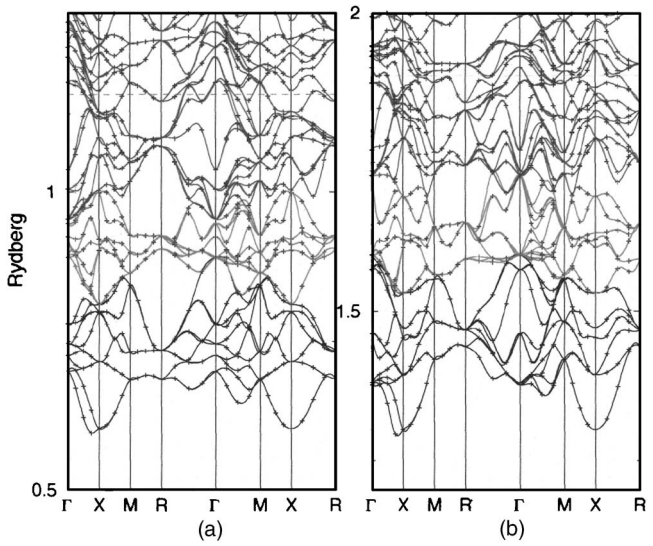

FIG. 11. Calculated band structures for $D0_3$ Mo_3Si, using (a) FP-LMTO with single-kappa basis and (b) TB method. Shown in the figure are Mo's 5*s*, (partial) 3*d*, and Si's 3*p* bands. The dashed lines are the Fermi levels.

IV. MONTE CARLO SIMULATION

In this section, we discuss Monte Carlo (MC) simulation based on the TB total energy scheme. Our goal is to predict CTEs for A15 Mo_3Si at various elevated temperatures. Calculating CTEs using MC simulation presents a numerical challenge, because the energy is near its minimum when the lattice constants are sampled. The lattice constant can fluctuate widely without suffering a large energy penalty.

The A15 Mo_3Si system simulated consists of 216 atoms ($3\times3\times3$ supercells). We set eight such systems at temperatures ranging from 1200 through 1900 K, incremented by 100 K. These systems are started from the same initial equilibrium configuration. At each MC step, we attempt to either displace a randomly selected atom, or change the lattice constant. After 100 000 MC steps, when all systems have achieved thermal equilibrium, lattice constants are sampled at every 20 MC steps. Five hundred samples are taken and averaged, and their temperature dependence is plotted in Fig. 12. For the specified temperature range, the material's thermal expansions are fairly linear. The CTEs can be easily read off from the figure, which is roughly about 9.0×10^{-6}/K.

To relate our theoretical work with experimental results, we have also simulated a $Mo_{53}Si$ system (i.e., one out of 54 Mo atoms in a bcc α-Mo is replaced by a Si atom), using the same set of parameters. Figure 13 shows the sampled average lattice constants at eight different temperature points. The data are compared with the experiment,[17] which was on a $Mo_{39}Si$ alloy (containing 2.5 at. % of Si). The reason we consider $Mo_{53}Si$ rather than $Mo_{39}Si$ is purely geometrical: $Mo_{53}Si$ can be easily realized using $3\times3\times3$ supercell. Our theoretical prediction of CTE for $Mo_{53}Si$ is about 5.0×10^{-6}/K, while the experimental CTE for $Mo_{39}Si$ is about 6.5×10^{-6}/K. Comparing to the published CTE result[18] for pure Mo, which is 4.2×10^{-6}–5.0×10^{-6}/K, we thus predict

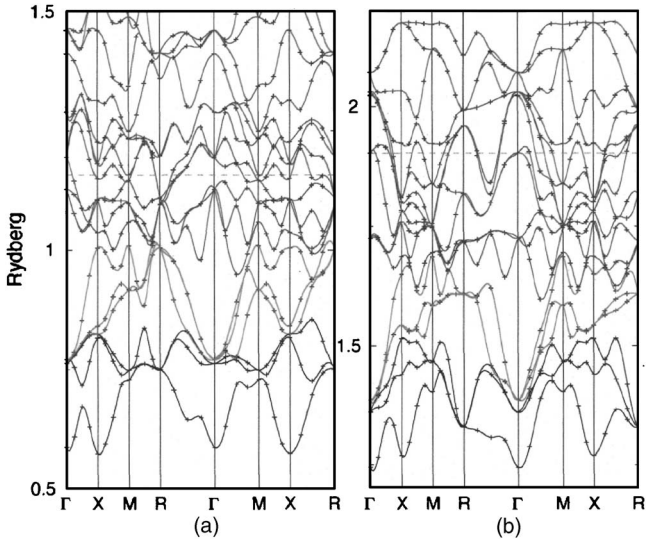

FIG. 10. Calculated band structures for $L1_2$ Mo_3Si, using (a) FP-LMTO with single-kappa basis and (b) TB method. Shown in the figure are Mo's 5*s*, (partial) 3*d*, and Si's 3*p* bands. The dashed lines are the Fermi levels.

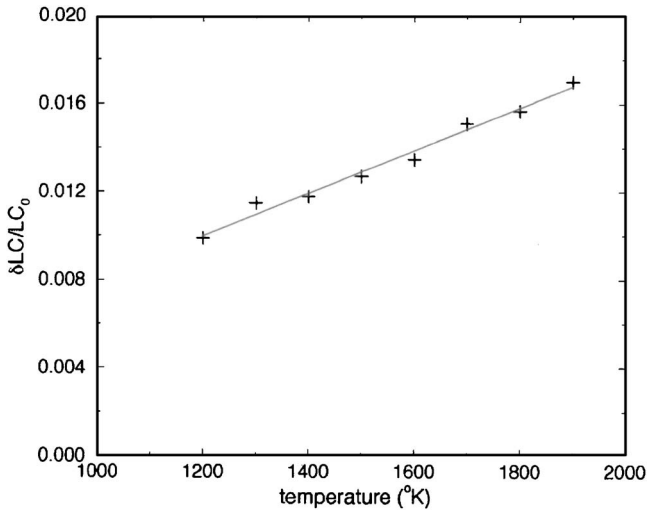

FIG. 12. The averaged change in lattice constants for Mo_3Si at eight temperature points. Data obtained from MC simulation.

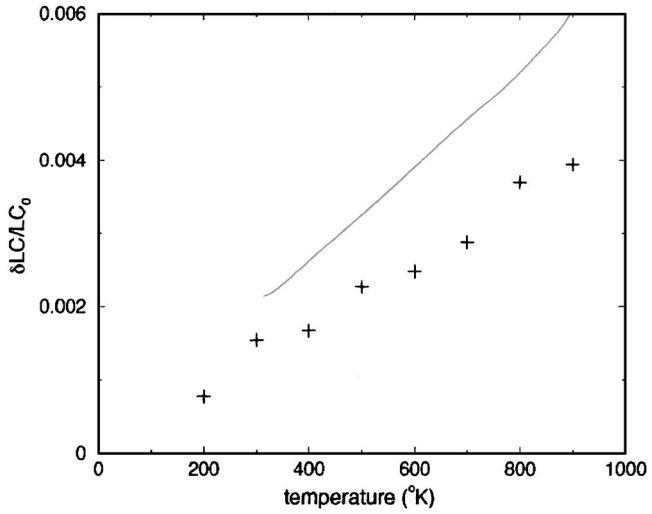

FIG. 13. Pluses: the averaged change in lattice constant for $Mo_{53}Si$ at various temperature, data obtained by MC simulation; solid curve: change of linear size for $Mo_{39}Si$, data obtained by experiment.

the trend that having a Si-rich compound causes larger CTE. Considering the error range associated with a typical MC method, the agreement of our theoretical prediction and experimental work is satisfactory.

V. SUMMARY

We modified McMahan's scheme of obtaining TB parameters directly from FP-LMTO calculations, and developed a set of TB parameters for A15 Mo_3Si. Our TB parameters are reasonably accurate for computing various static properties, and quite transferable for close-packed structures. We used these parameters in MC simulation to compute the CTEs of Mo_3Si and $Mo_{53}Si$. The result of the latter material is in good agreement with our experiments.

ACKNOWLEDGMENTS

This work is sponsored by the Office of Fossil Energy, Advanced Research Materials (ARM) Program, U.S. Department of Energy, under Subcontract No. 4000013127 with Oak Ridge National Laboratory (ORNL) managed by UT-Battelle, LLC. We thank Dr. David Djajaputra for his codes for anti-Fourier transforming LMTO matrices, and Dr. Leonoid Muratov for his advice and guidance in using the FP-LMTO technique.

[1] J. C. Slater and G. F. Koster, Phys. Rev. **94**, 1498 (1954).
[2] D. A. Papaconstantopoulos, *Handbook of the Band Structure of Elemental Solids* (Plenum, New York, 1986).
[3] D. A. Papaconstantopoulos and M. J. Mehl, Phys. Rev. B **54**, 4519 (1996); S. H. Yang, M. J. Mehl, and D. A. Papaconstantopoulos, *ibid.* **57**, R2013 (1998).
[4] D. A. Papaconstantopoulos and M. J. Mehl, Phys. Rev. B **64**, 172510 (2001); S. H. Yang, M. J. Mehl, and D. A. Papaconstantopoulos, J. Phys.: Condens. Matter **14**, 1895 (2002).
[5] A. K. McMahan and J. E. Klepeis, Phys. Rev. B **56**, 12250 (1997).
[6] A. K. McMahan and J. E. Klepeis, Mater. Res. Soc. Symp. Proc. **491**, 199 (1998).
[7] D. L. Price and B. R. Cooper, Phys. Rev. B **39**, 4945 (1989); D. L. Price, J. M. Wills, and B. R. Cooper, *ibid.* **46**, 11368 (1992).
[8] D. Djajaputra and B. R. Cooper, Phys. Status Solidi B **236**, 97 (2003).
[9] O. K. Andersen and O. Jepsen, Phys. Rev. Lett. **53**, 2571 (1984).
[10] Th. Frauenheim, F. Weich, Th. Köhler, S. Uhlmann, D. Porezag, and G. Seifert, Phys. Rev. B **52**, 11492 (1995); J. Widany, Th. Frauenheim, Th. Köhler, M. Sternberg, D. Porezag, G. Jungnickel, and G. Seifert, *ibid.* **53**, 4443 (1996).
[11] C. L. Briant, Mater. Res. Soc. Symp. Proc. **322**, 461 (1994).
[12] J. H. Schneibel, C. T. Liu, D. S. Easton, and C. A. Carmichael, Mater. Sci. Eng., A **261**, 78 (1999); I. Rosales and J. H. Schneibel, Intermetallics **8**, 885 (2000); H. Choe, D. Chen, J. H. Schneibel, and R. O. Ritchie, *ibid.* **9**, 209 (1994); J. H. Schneibel, C. J. Rawn, T. R. Watkins, and E. A. Payzant, Phys. Rev. B **65**, 134112 (2002).
[13] R. E. Cohen, M. J. Mehl, and D. A. Papaconstantopoulos, Phys. Rev. B **50**, 14694 (1994).
[14] C. Z. Wang, B. C. Pan, M. S. Tang, H. Haas, M. Sigalas, G. D. Lee, and K. M. Ho, Mater. Res. Soc. Symp. Proc. **491**, 211 (1998).
[15] M. S. Daw, S. M. Foiles, and M. I. Baskes, Mater. Sci. Rep. **9**, 251 (1992).
[16] M. J. Mehl, J. E. Osburn, D. A. Papaconstantopoulos, and B. M. Klein, Phys. Rev. B **41**, 10311 (1990).
[17] N. Ma, B. R. Cooper, and B. S. Kang, Office of Fossil Energy, Advanced Research Material Programs, U.S. Department of Energy Topical Report No. 4000013127, 2003 (unpublished).
[18] F. C. Nix and D. MacNair, Phys. Rev. **61**, 74 (1942).